Effect of phase separation on the Jian ware blue colored glaze with iron oxide

Pei Shi, Fen Wang*, Jianfeng Zhu, Biao Zhang, Ting Zhao, Yi Wang, Jiahuan Wang

School of Materials Science and Engineering, Shaanxi University of Science & Technology, Xi'an 710021, PR China

A B S T R A C T

This study was aimed to explore the effect of phase separation on the Jian ware blue colored glaze with iron oxide. In order to analyze the forming cause of glaze patterns and their coloring mechanism, the phase, microstructure and chemical state of the samples were investigated by X-ray diffraction, scanning electron microscopy, transmission electron microscopy and X-ray photoelectron spectrum. The results indicated that the addition of calcium phosphate introduced highly-active Ca^{2+} and P^{5+} into the glaze. Since Ca^{2+} with high ionic potential had a greater ability to appeal O^{2-} than Si^{4+}, the glaze melt was separated into calcium-rich phase and silicon-rich phase. The difference of viscosity caused the non-uniform distribution of quartz and glass phase, and then affected the distribution of iron ions in two phases, which formed glaze patterns. Adding P^{5+} that had a strong effect of reversed polarization on the Fe-O increased the contents of Fe^{2+} and Fe^{3+}-O-Fe^{2+}, and thus deepened the blue-green of glaze surface. In addition, it promoted the formation of worm-like phase-separated structures and the existence of structural color. Therefore, phase separation enriched not only patterns but also glaze colors of the Jian ware blue colored glaze.

1. Introduction

Liquid immiscibility of glasses is designated as phase separation. It exists in many compositions that consist of silicate, borate, phosphate, alkaline metal oxides, alkaline earth metal oxides and transitional metal oxides. The phase separation plays an important role in formation of the nuclei so as to prepare various high-performance glassy materials [1,2]. More importantly, being similar to the crystallization [3], the phase separation also has a profound influence on the artistic appearance of glazes.

Jian bowls are well known for their spectacular streaked or mottled patterns. The most common and famous variety, called "Hare's fur" (HF), is a shining black glaze showing fine radial rust-colored streaks. The Hare's fur was believed to originate from phase separation of glaze melt and crystallization of iron oxides. At high temperatures, the phase-separation droplets of rich iron were formed and aggregated in the glaze surface by the surface tension and weight, and then the crystals of iron oxides precipitated from droplets and formed surface patterns [4–6]. Similarly, the phase separation and crystallization were also the forming reason of red flowers in the iron-red glaze [7]. Besides, the Jun and Ru wares' opalescence blue was known as the result of the phase separation. The opalescence blue refers to beautiful sky-green and opacifying state, as the green agate or Yuhua stone. When the average diameter of phase-separation droplets was 1–100 nm, the opalescence blue was formed in the glaze surface, contributing to the coloring of iron ions [8,9]. Moreover, inspired by amorphous photonic crystals of the biological world, Yin et al. proposed that the structural color of amorphous photons could be formed in the glaze, when the phase-separated structures were in short range order with average diameter of 106–260 nm [10,11]. However, in addition to the patterns of iron oxides crystals and the structural color, there are few researches about the formation of other surface appearances by phase separation, such as the Jian ware blue colored glaze.

In the production of ancient ceramics, phosphorus was introduced by burning animal bones and plants, whereas it could cause environmental pollution [12]. Therefore, we attempted to use calcium phosphate instead of them as the phase-separative promoter to prepare the Jian ware blue colored glaze with iron oxide. Effects of calcium phosphate on the glaze color, chemical composition and microstructure of the iron glazes were investigated, aiming at analyzing the formation and coloration mechanisms of the Jian ware blue colored glaze. This work will throw some light on the preparation of ceramic glazes with different artistic effects.

Table 1
Chemical compositions of the mineral raw materials (wt%).

Raw materials	SiO_2	Al_2O_3	Fe_2O_3	CaO	MgO	K_2O	Na_2O	TiO_2
Feldspar	74.68	15.50	0.08	–	0.07	6.03	3.64	–
Quartz	98.43	0.22	0.04	0.53	0.67	0.04	0.07	–
Calcite	1.58	–	0.07	96.80	1.19	–	0.36	–
Talc	65.50	–	0.14	0.92	33.34	–	–	0.10
Kaolin	60.00	37.62	0.23	0.09	–	0.42	1.49	0.15

2. Experimental procedure

2.1. Materials

The base glaze compositions were made by 60 wt% feldspar, 24 wt% quartz sand, 12 wt% calcite, 2 wt% talc and 2 wt% kaolin. Meanwhile, 0–4 wt% calcium phosphate ($Ca_3(PO_4)_2$, analytical reagent) was added as the phase-separative promoter and 4 wt% iron oxide (Fe_2O_3, analytical reagent) was used as the colorant. It needed to be emphasized that the chemical compositions of samples did not completely copy the ancient Jian ware blue colored glaze. The chemical compositions of mineral raw materials are given in Table 1.

2.2. Glaze preparation

The glaze slip was prepared by directly milling the starting materials with 75 wt% water, 0.8 wt% sodium carboxyl methyl cellulose (CMC) and 0.3 wt% sodium tripolyphosphate (STP) at a rate of 300 r/min for 40 min. Then it was sieved and the density was adjusted to 1.5 g/cm^3 by water. By dipping, the glaze slip was applied to the biscuit firing pieces (Ø 2–3 cm). After dried, the test pieces were fired at a heating rate of 3 °C/min to 900 °C and 1.5 °C/min to 1250 °C, and then held 40 min at this temperature under an oxidizing atmosphere. Finally, the samples were cooled down to room temperature naturally in the muffle furnace.

2.3. Characterization techniques

The ultraviolet-visible-NIR (UV–vis–NIR) spectrum at room temperature was performed on a Cary 5000 spectrometer. The crystalline phases were identified by X-ray diffraction analysis (XRD, D/max 2200PC, Rigaku, Japan) using Cu-Kα radiation (λ = 1.5406 Å). XRD patterns were recorded at room temperature with a step size of 0.02° in 10–50° 2θ range. The microstructures of the samples were characterized by scanning electron microscopy (SEM, Hitachi S-4800, Japan) and transmission electron microscopy (TEM, Tecnai G2 F20, America) operated at 15 kV and 200 kV, respectively. Before the testing stage, the sample for SEM was etched using 1 vol% HF for 40 s to expose crystals and phase separation structures, and the sample for TEM did not required to etch. Analysis of the X-ray photoelectron spectrum (XPS) was performed on an AXIS SUPRA spectrometer.

3. Results and discussion

Fig. 1 shows the surface appearances and corresponding UV–vis reflectance spectra of the glazes without and with 4 wt% $Ca_3(PO_4)_2$. As shown in Fig. 1(a) and (c), the glaze without $Ca_3(PO_4)_2$ exhibited the original color of Fe_2O_3, whereas the glaze with 4 wt% $Ca_3(PO_4)_2$ was similar to the Jian ware blue colored glaze that had abundant colors and patterns. From Fig. 1(b), a wide reflectance peak corresponding to brown appeared in the spectrum of the sample without $Ca_3(PO_4)_2$. Besides, the spectrum of the glaze with 4 wt% $Ca_3(PO_4)_2$ had two reflection peaks at 441 and 526 nm (Fig. 1(d)). The first peak corresponded to blue, while the other was green.

To further study the effect of $Ca_3(PO_4)_2$ on the glaze appearance, the crystallization behavior was investigated in detail. Fig. 2 presents the
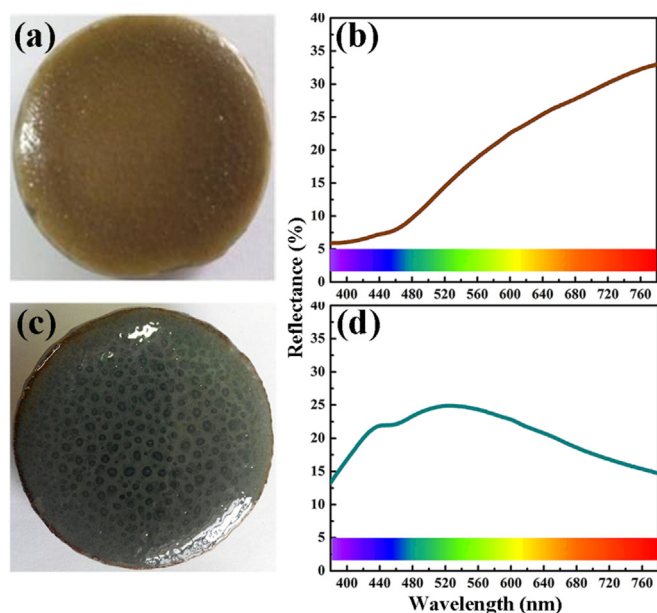
Fig. 1. Appearance and UV–vis reflectance spectra of the typical glazes with Fe_2O_3, (a)-(b) 0 $Ca_3(PO_4)_2$; (c)-(d) 4 wt% $Ca_3(PO_4)_2$.
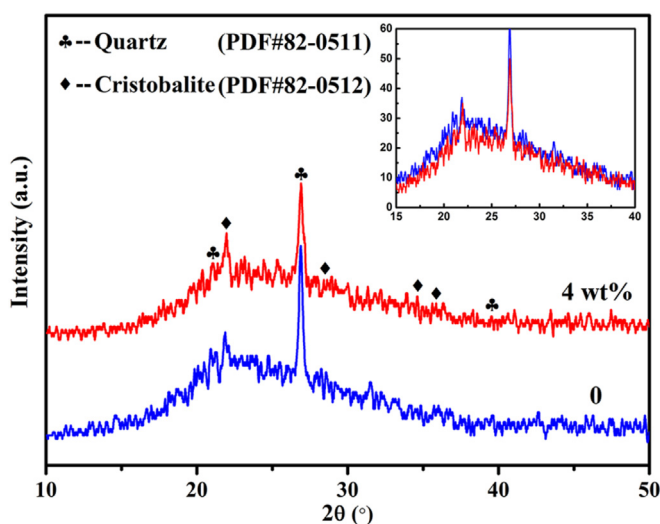
Fig. 2. XRD patterns of the glazes with different $Ca_3(PO_4)_2$ contents.

XRD patterns of the samples with different $Ca_3(PO_4)_2$ contents. Diffraction lines of the two samples were superimposed on a diffuse hump, indicating a high amount of glass phase. Meanwhile, the enlarged figure of the 2θ ≈ 15–40° range showed that their contents were similar. Despite the difference in $Ca_3(PO_4)_2$ contents, the main crystalline phase of the glazes was only quartz (SiO_2, PDF#82–0511). And the minor crystalline phase of cristobalite (SiO_2, PDF#82–0512) was also detected in the samples. Addition of $Ca_3(PO_4)_2$ to the glaze, the intensity of the quartz peaks decreased obviously. Therefore, $Ca_3(PO_4)_2$ could not promote the formation of glass phase, whereas it benefited to the melt of quartz.

SEM images of the etched glaze surface without $Ca_3(PO_4)_2$ are shown in Fig. 3. From Fig. 3(a)-(c), a large number of cubic crystals distributed disorderly in the glaze surface. The chemical composition of the crystals was analyzed by EDS in Fig. 3(d). It showed that the crystal was rich in Si and O. By combining with the quantity and chemical composition of cubic crystals, they could only be quartz.

Fig. 4 displays the SEM and EDS images of the etched glaze surface with 4 wt% $Ca_3(PO_4)_2$. As revealed in Fig. 4(a), the light colored area
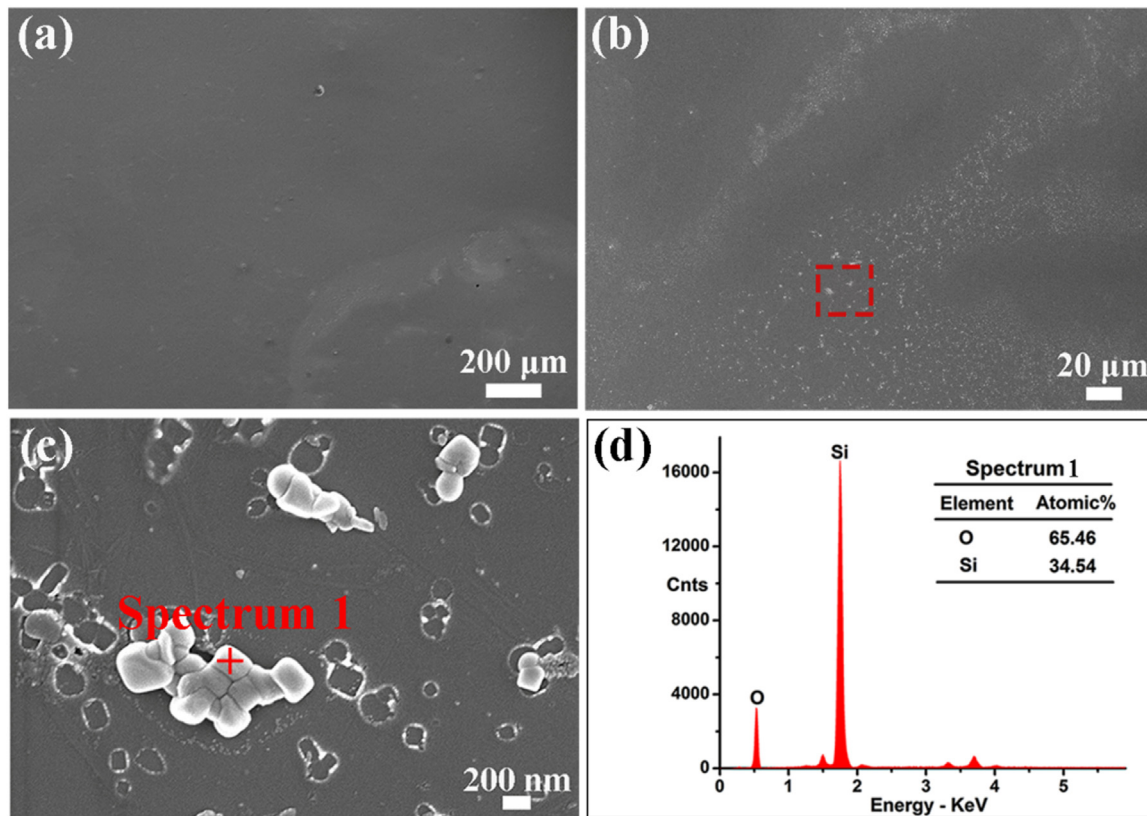
Fig. 3. (a)-(b) SEM images of the etched glaze surface without $Ca_3(PO_4)_2$; (c) Enlarged image of (b); (d) EDS spectrum of crystal 1.

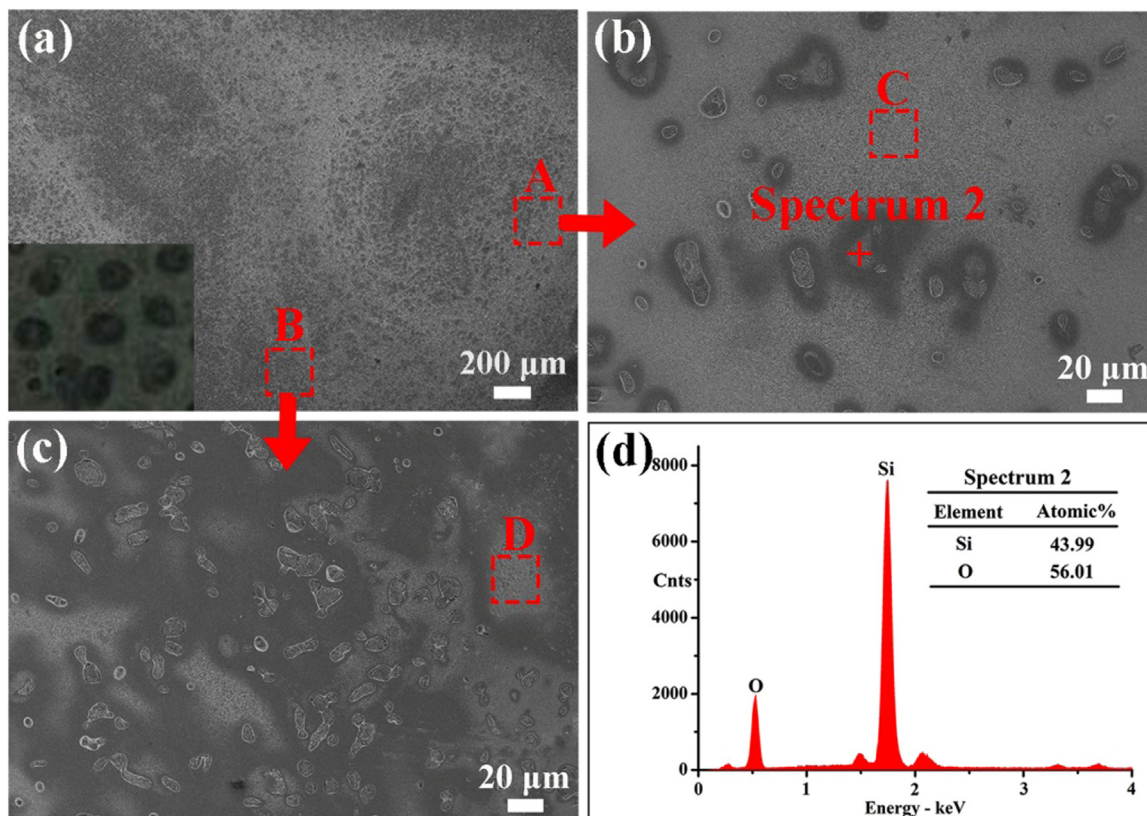**Fig. 4.** (a) SEM image of the etched glaze surface with 4 wt% $Ca_3(PO_4)_2$; (b)-(c) Enlarged images of A and B; (d) EDS spectrum of crystal 2. (The data about C and D were discussed later in Fig. 9 description).
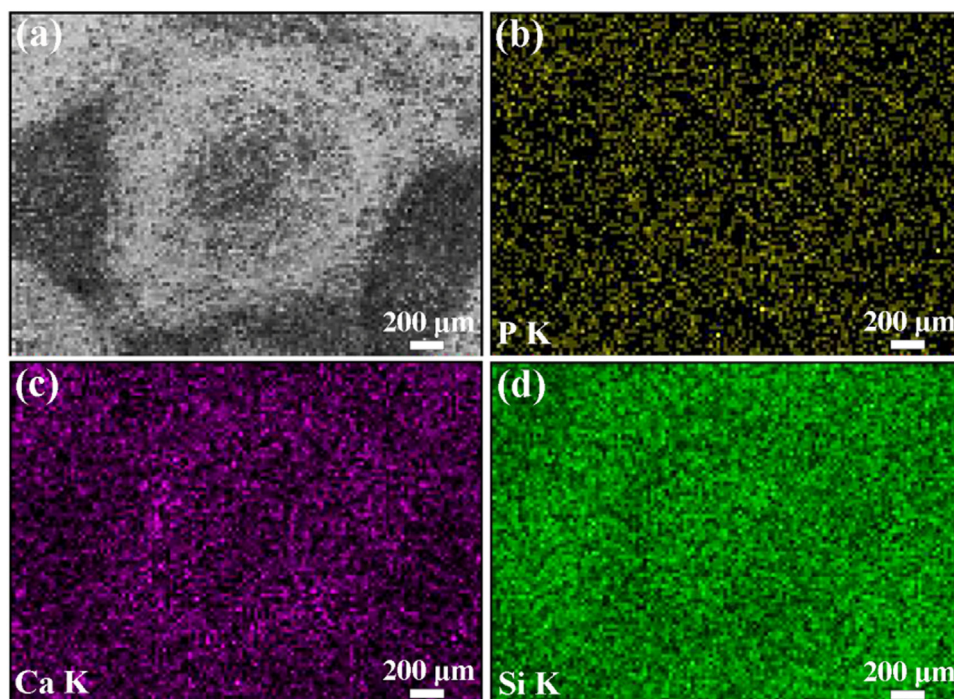
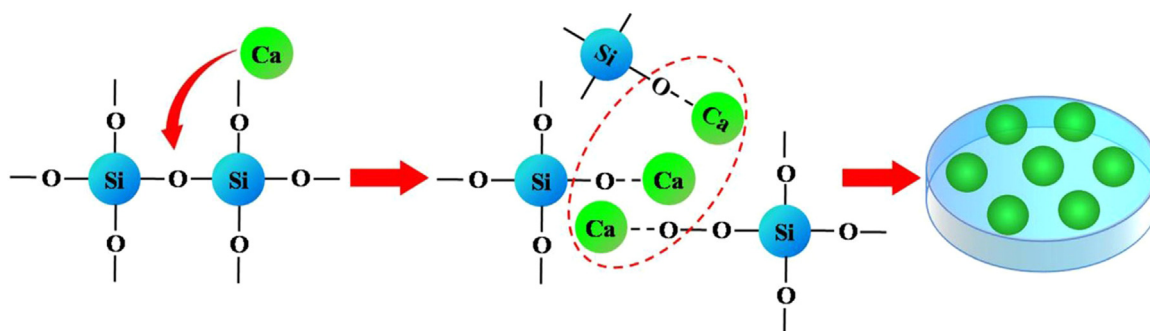**Fig. 5.** SEM image and elemental mapping images of the pattern for the sample with 4 wt% $Ca_3(PO_4)_2$.

Fig. 6. Schematic diagram of forming patterns in the $Ca_3(PO_4)_2$ sample.

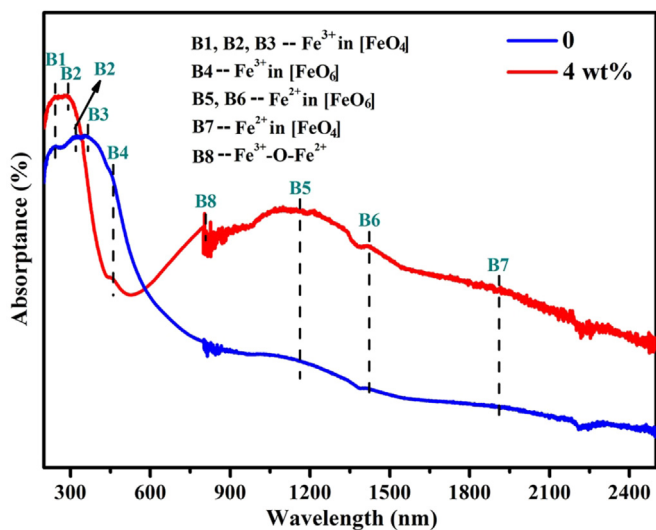**Fig. 7.** UV–vis–NIR absorption spectra of the glazes with different $Ca_3(PO_4)_2$ contents.

(A) corresponded to the glaze pattern, and the dark colored area (B) corresponded to the gap between patterns. Additionally, from Fig. 4(b) and (c), some aggregate crystals were observed on the glaze surface. For comparison, the crystal content of A was less than that of B, indicating more glass phase existed in the glaze pattern than the gap. Fig. 4(d) presents the EDS analysis of crystals. Apparently, they were rich in Si and O. According to the XRD and EDS results, the aggregate crystals were quartz. Generally, the chemical color formed by colorant plays an important role in the glaze. From Fig. 2, there was no crystallization of iron, so iron was mainly in the form of ions in the glass phase. As shown in Fig. 4(b) and (c), the more the crystal was, the less the glass phase and iron ions were in the glaze surface. Hence, the color of glaze pattern was dark, and the color of gap between patterns was light. What caused the uneven distribution of quartz?

Fig. 5 shows the SEM/EDS elemental analysis of the pattern in Fig. 4(a). Uniform P, strong Ca and weak Si signals were detected from the pattern, indicating that the uneven distribution of quartz was closely related to Ca. In general, modifiers (Na_2O, K_2O, CaO, MgO) break up the silica network if the O:Si ratio increases significantly. In this case, modifiers cations always try to attract non-bridging oxygen ions in terms of their arrangements. When modifiers cations have high ionic potential, the free energy of glass system is too high, so the thermodynamic stable and homogeneous glass could not be formed. They
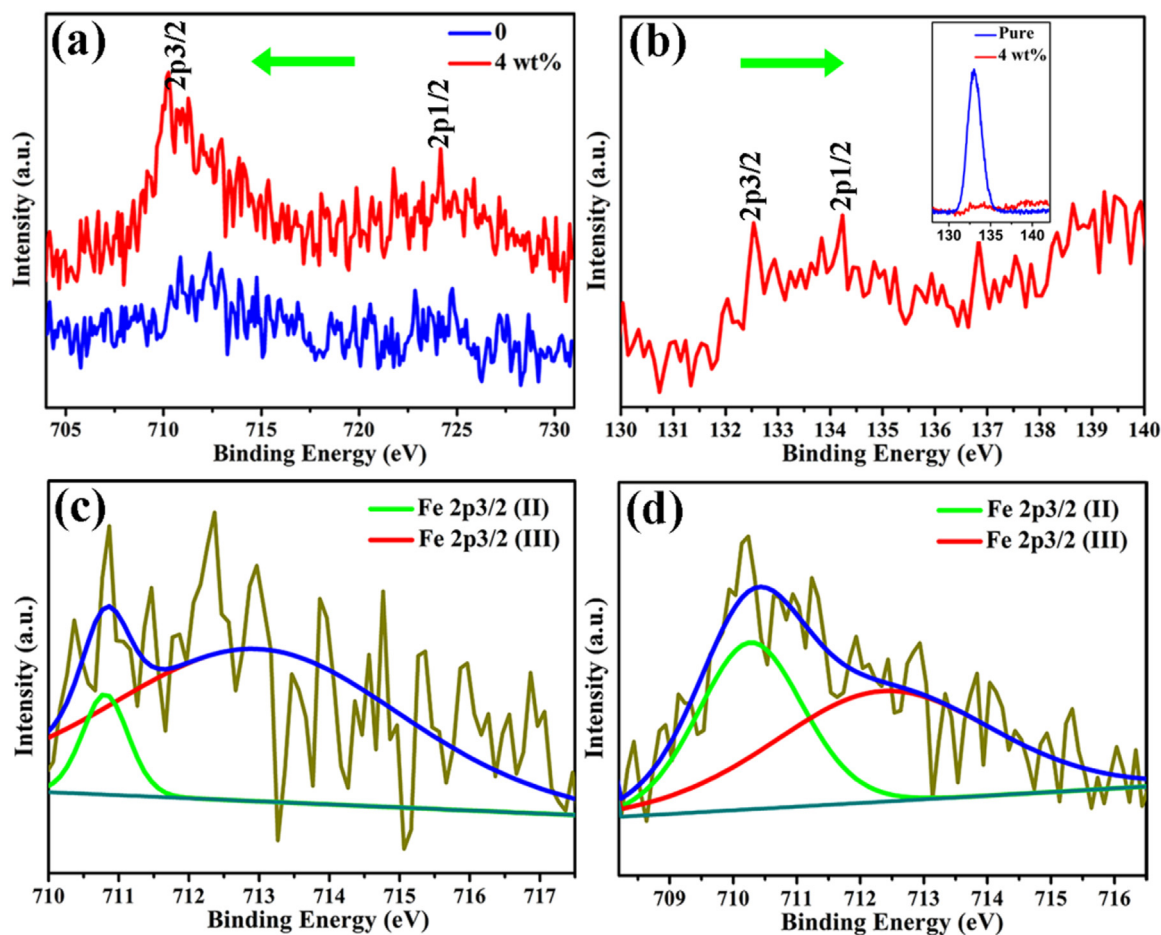
4

Fig. 8. (a) XPS spectra of Fe 2p for the samples; (b) XPS spectra of P 2p for the pure $Ca_3(PO_4)_2$ and the sample with 4 wt% $Ca_3(PO_4)_2$; (c)-(d) Fitting XPS spectra of Fe 2p3/2 for the samples with 0 and 4 wt% $Ca_3(PO_4)_2$.

spontaneously separate from the silica network and form self-contained system. One phase is rich in alkali, and the other is rich in silicon [13]. By adding $Ca_3(PO_4)_2$, Ca^{2+} content increased in the glaze. Since the ionic potential of Ca^{2+} was 1.89, it had strong competition ability in obtaining O^{2-}, causing the phase separation of glaze melt at high temperatures. Since the surface tension of calcium-rich phase was greater than that of the silicon-rich phase, circular patterns were formed on the surface of sample after natural cooling. The schematic diagram is shown in Fig. 6.

According to the theory of crystal nucleation and growth, the quartz of calcium-rich phase was easier to grow, while silicon-rich phase tended to form more and smaller quartz crystals. As a result, quartz was not evenly distributed on the surface of the $Ca_3(PO_4)_2$ sample, which formed dark patterns. Meanwhile, dense crystals in the gap increased the opacity and deepened the opal effect of glaze surface. In addition, according to the Na_2O-CaO-SiO_2 phase equilibrium diagram, the increase of CaO content decreased the crystallization of quartz, whereas the glass phase content did not change fundamentally at the same firing temperature (Fig. 2) [14].

Fig. 7 shows the UV–vis–NIR absorption spectra of the glazes with 0 and 4 wt% $Ca_3(PO_4)_2$. In the spectrum of the glaze without $Ca_3(PO_4)_2$, the absorption peaks were found at 241, 318, 359, 462, 1180, 1418 and 1907 nm. Fe^{3+} in $[FeO_4]$ tetrahedron presented three intense charge transference bands around 241, 318 and 359 nm [15]. And the shoulder peak at 462 nm associated to $^6A_{1g}(S) \rightarrow {}^4A_{1g}$, $^4E_g(G)$ forbidden transition of Fe^{3+} in $[FeO_6]$ octahedron. Besides, there were two strong absorption bands at 1180 and 1907 nm in the samples. They corresponded to the characteristic absorption bands of Fe^{2+} in $[FeO_6]$ octahedron and

$[FeO_4]$ tetrahedron, respectively. Meanwhile, the shoulder peak at 1418 nm was related to the deformation of $[FeO_6]$ octahedron structure of Fe^{2+} [15,16]. The similar bands were also observed in the spectrum of the glaze containing 4 wt% $Ca_3(PO_4)_2$. Except for these peaks, the absorption peak at 804 nm were found in the $Ca_3(PO_4)_2$ sample. Zhang et al. [17] investigated that Fe^{3+}-O-Fe^{2+} (the structure of Fe_3O_4) exhibited a strong characteristic peak in near infrared region that was close to the visible light region in the glass colored with Fe_2O_3. Thus, the peak at 804 nm corresponded to the characteristic absorption of Fe^{3+}-O-Fe^{2+}. With the addition of $Ca_3(PO_4)_2$, the intensity of characteristic peaks of Fe^{2+} increased, while a small amount of Fe^{3+} existed in the form of $[FeO_6]$ octahedron. Therefore, addition of $Ca_3(PO_4)_2$ to the glaze colored with Fe_2O_3 might contribute to the reduction of Fe^{3+} and the formation of Fe^{3+}-O-Fe^{2+}.

The chemical states of the glazes with different $Ca_3(PO_4)_2$ contents were further analyzed by XPS. From Fig. 8(a), for the Fe 2p in the sample without $Ca_3(PO_4)_2$, the peaks at 712.3 and 724.7 eV were assigned to Fe 2p3/2 and Fe 2p1/2 [18,19]. But in the spectrum of the glaze adding 4 wt% $Ca_3(PO_4)_2$, the peak values of Fe 2p shifted to 710.2 and 724.1 eV, a slightly lower than the glaze without $Ca_3(PO_4)_2$. Furthermore, the opposite tendency was exhibited in the P 2p which the binding energy values were observed at 132.6 and 134.2 eV in the glaze with $Ca_3(PO_4)_2$, a slightly higher than that of the pure $Ca_3(PO_4)_2$ (132.1 and 133.3 eV, seen in Fig. 8(b)) [20,21]. Such chemical shifts for Fe 2p and P 2p might originate from the interaction between Fe_2O_3 and $Ca_3(PO_4)_2$. In detail, the electronegativity value of Fe element is 1.83, a little smaller than that P element of 2.19. After introducing $Ca_3(PO_4)_2$ into the glaze colored with Fe_2O_3, the electron density of Fe should get
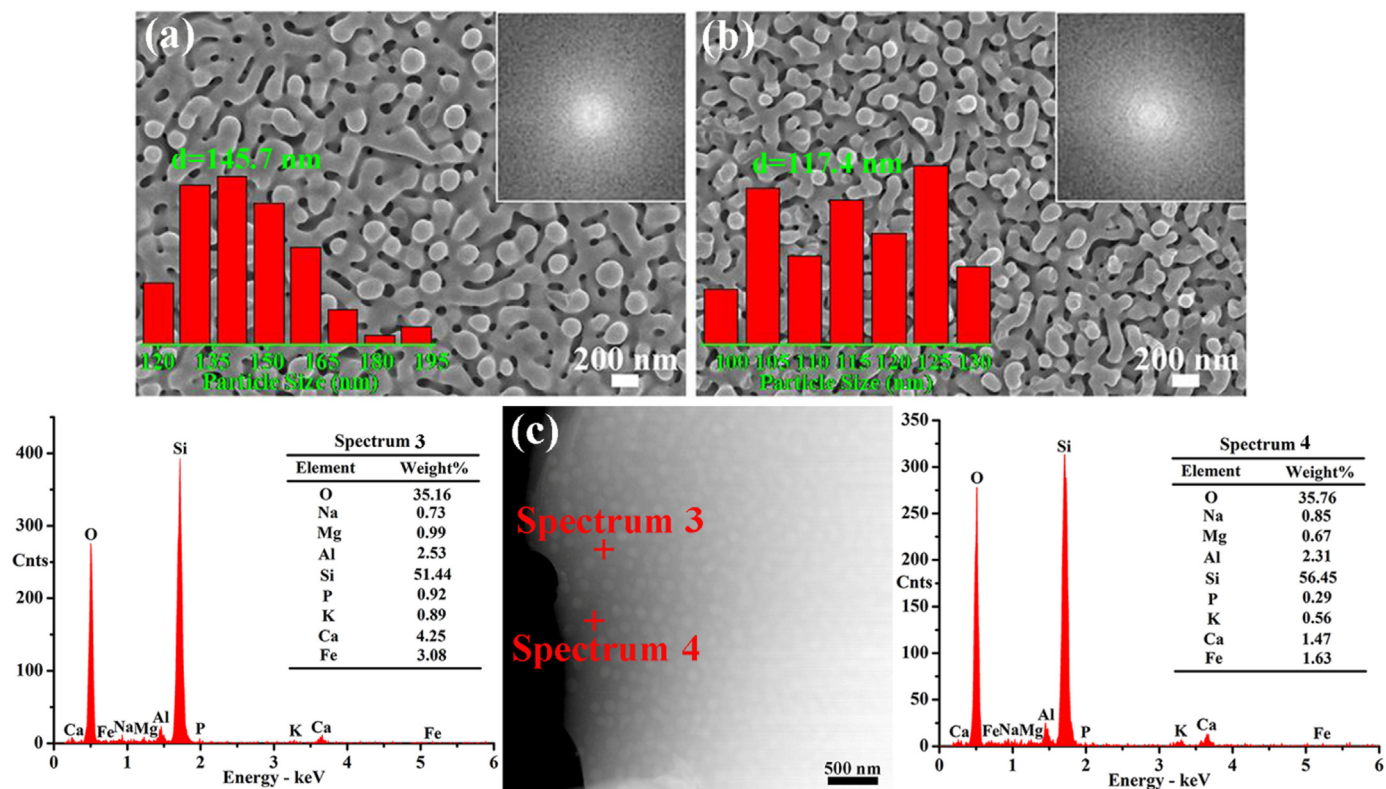
Fig. 9. SEM, STEM images and corresponding EDS spectra of the glaze with 4 wt% $Ca_3(PO_4)_2$, (a) and (b) enlarged images of C and D in Fig. 4; (c) STEM image and EDS spectra of point 3 and 4 in the pattern.

Table 2
Calculation factor of refractive index about oxide component in the glass composition.

Oxide component	Na_2O	MgO	Al_2O_3	SiO_2	P_2O_5	K_2O	CaO	Fe_2O_3
n_i	1.590	1.625	1.520	1.460	1.435	1.575	1.730	3.010

weak by the attraction of P and result in the increase of electron polarization of Fe-P. Actually, the electron density of Fe was enhanced with the addition of $Ca_3(PO_4)_2$. Since P^{5+} had a strong effect of reversed polarization on the Fe-O, the corresponding values of Fe 2p shifted to a lower energy region, while the P 2p to a higher energy region [15,22–24].

Fig. 8(c) and (d) shows the fitting Fe 2p3/2 spectrums of the samples. In the fitting spectrum of the glaze without $Ca_3(PO_4)_2$, two peaks at 710.8 and 712.9 eV were observed, which were ascribed to Fe 2p3/2(II) and Fe 2p3/2(III). In addition, the peaks of Fe 2p3/2(II) and Fe 2p3/2(III) located at 710.3 and 712.4 eV in the glaze with 4 wt% $Ca_3(PO_4)_2$. Based on the relative peak area, the atomic ratios of Fe^{2+} and Fe^{3+} in the two samples were 10:90 and 42:58, respectively. Therefore, the reversed polarization of Fe-O increased the Fe^{2+} content.

According to the theory of coordination chemistry [15], Fe^{3+} in silicate glass mainly existed as $[FeO_4]$ tetrahedron similar to $[SiO_4]$ tetrahedron. With the introduction of P, most of Fe^{3+} in $[FeO_4]$ tetrahedron transformed into Fe^{2+} and small amount of Fe^{3+} in $[FeO_6]$ octahedron. Meanwhile, Fe^{2+} in $[FeO_6]$ octahedron broke up the rest of $[FeO_4]$ tetrahedron structure of Fe^{3+}, and then linked with Fe^{3+}-O. Consequently, Fe^{3+}-O-Fe^{2+} was formed in the $Ca_3(PO_4)_2$ glaze. Since Fe^{2+} and Fe^{3+}-O-Fe^{2+} contributed to deepening the blue green of glaze surface, adding $Ca_3(PO_4)_2$ changed the glaze color from brown to dark cyan.

The enlarged figures of the two glass phases at glaze pattern (C) and gap between patterns (D) in Fig. 4(b) and (c) are shown in Fig. 9(a) and (b). Apparently, the worm-like phase-separated structures were formed in the C and D. The structure unit of silicate glasses was $[SiO_4]$ tetrahedron. With the addition of $Ca_3(PO_4)_2$, P^{5+} of high charge state and field strength was introduced to the silicate glass, which increased the free energy of system and decreased the stability of glass. Hence, the phase separation was carried out in the whole glaze. In the system of low viscosity, the phase-separated structures were easier to grow, so the average size in the glaze pattern was larger than that of the gap. Insets of Fig. 9(a) and (b) present the corresponding 2D FFT images and the particle size distribution charts. The ring-shaped 2D FFT images and the average diameter of 106–260 nm indicated that the worm-like phase separation structures belonged to the amorphous photons structure [10,11].

The STEM image and EDS spectra in Fig. 9(c) revealed the chemical compositions of two phases in the pattern. Apparently, Ca, P, and Fe were mainly enriched in the microphase, and the matrix was rich in Si. The refractive index of glass is calculated by using sum over states formula [25].

$$n = n_1 p_1 + n_2 p_2 + ... + n_i p_i \tag{1}$$

In this expression, p is the mole fraction of oxide in chemical compositions, and n_i is the refractive index calculation factor of oxide component, as shown in Table 2. According to the Eq. (1), the refraction index of the base phase (n_{Si}) was 1.512, and the microphase (n_P) was 1.554. Furthermore, we applied the Maxwell-Garnett equation to calculate the effective refractive index (n_e) of the phase-separation glaze, where φ was the volume fraction of microphase [26].

$$n_e = n_{Si} \left(\frac{2n_{Si}^2 + n_P^2 + 2\varphi(n_P^2 - n_{Si}^2)}{2n_{Si}^2 + n_P^2 - \varphi(n_P^2 - n_{Si}^2)} \right)^{1/2} \tag{2}$$

Based on the Eq. (2), the theoretical calculation of n_e was 1.550 with assuming $\varphi = 90\%$. The approximate expression for the scattering light wavelengths of the amorphous photons crystals is given by the modified

form of Bragg's law:

$$\lambda = 2dn_e \qquad (3)$$

The theoretical calculation of λ was 453 nm with $d = 145.7$ nm and $n_e = 1.550$ by Eq. (3), which was within the range of blue light wavelength (435–480 nm) [27]. Hence, the blue appeared in the glaze surface with 4 wt% $Ca_3(PO_4)_2$. The coupling action between structural color and chemical color enriched the coloring effect of phase separation glaze [11].

4. Conclusion

The glazes without and with 4 wt% $Ca_3(PO_4)_2$ were compared and analyzed to establish the relationships between the phase separation and the Jian ware blue colored glaze with iron oxide. According to the SEM/EDS results, the addition of $Ca_3(PO_4)_2$ introduced the Ca^{2+} of high ionic potential into the glaze, so that the glaze melt separated into alkali-rich and silicon-rich phases at high temperatures. In the low viscosity alkali-rich phase, the less quartz precipitated, the more glass phase and iron ions existed. Hence, the dark patterns were formed in the glaze surface. The XPS analysis showed adding $Ca_3(PO_4)_2$ also introduced P^{5+} that had a strong effect of reversed polarization on the Fe-O. Thus, Fe^{2+} and Fe^{3+}-O-Fe^{2+} contents increased and blue-green of the glaze surface deepened. Besides, the introduction of P^{5+} promoted the formation of worm-like phase-separated structures, making it possible to appear the structural color of amorphous photons in the glaze surface. The structural color modified the chemical color of Fe_2O_3 and enriched the glaze appearance.

Acknowledgements

References

[1] A. Yasumori, Preparation of functional glasses and glass ceramics using stable immiscibility, J. Ceram. Soc. Jpn. 121 (2013) 471–479.

[2] C. Hermansen, X.J. Guo, R.E. Youngman, J.C. Mauro, M.M. Smedskjaer, Y.Z. Yue, Structure-topology-property correlations of sodium phosphosilicate glasses, J. Chem. Phys. 143 (2015) 26162–28684.

[3] J.F. Zhu, P. Shi, F. Wang, T. Zhao, H. Jiang, Preparation of separative-phase fancy glaze derived from iron ore slag, Ceram. Int. 42 (2016) 5250–5257.

[4] C. Dejoie, P. Sciau, W.D. Li, L. Noé, A. Mehta, K. Chen, H.J. Luo, M. Kunz, N. Tamura, Z. Liu, Learning from the past: rare ε-Fe$_2$O$_3$ in the ancient black-glazed Jian (Tenmoku) wares, Sci. Rep. 4 (2014) 4941.

[5] W.D. Li, H.J. Luo, J.N. Li, J.Z. Li, J.K. Guo, Studies on the microstructure of the black-glazed bowl sherds excavated from the Jian kiln site of ancient China, Ceram. Int. 34 (2008) 1473–1480.

[6] C.Y. Chiang, H.F. Greer, R.S. Liu, W.Z. Zhou, Formation, crystal growth and colour appearance of Mimetic Tianmu glaze, Ceram. Int. 42 (2016) 7506–7513.

[7] X.Q. Chen, R.F. Huang, J. Sun, S.P. Chen, M.L. Ruan, D.F. Zhao, J.T. Wang, Morphology of multiple liquid phase separation in iron oxide red glaze and chemical composition of various phases, J. Chin. Ceram. Soc. 12 (1984) 108–114.

[8] F. Wang, H.J. Luo, Q. Li, W.D. Li, Characteristic and coloring mechanism of the separative-phase colored ceramic, J. Chin. Ceram. Soc. 37 (2009) 181–186.

[9] W.D. Li, J.Z. Li, Z.Q. Deng, J. Wu, J.K. Guo, Study on Ru ware glaze of the Northern Song dynasty: one of the earliest crystalline-phase separated glazes in ancient China, Ceram. Int. 31 (2008) 487–494.

[10] H.W. Yin, Study on the coloring mechanism and preparation method of structural color, Fudan University, Shanghai, 2008.

[11] P. Shi, F. Wang, J.F. Zhu, H.B. Yang, Y. Wang, Y. Fang, B. Zhang, J.H. Wang, Amorphous photonic crystals and structural colors in the phase separation glaze, J. Eur. Ceram. Soc. 38 (2018) 2228–2233.

[12] P. Sciau, L. Noé, P. Colomban, Metal nanoparticles in contemporary potters' master pieces: lustre and red "pigeon blood" potteries as models to understand the ancient pottery, Ceram. Int. 42 (2016) 15349–15357.

[13] Y. Li, H.H. Sun, X.M. Liu, Z.D. Cui, Effect of phase separation structure on cementitious reactivity of blast furnace slag, Sci. China Ser. E 52 (2009) 2695–2699.

[14] W.D. Li, J.Z. Li, Z.Q. Deng, J. Wu, J.K. Guo, Study on Ru ware glaze of the Northern Song dynasty: one of the earliest crystalline-phase separated glazes in ancient China, Ceram. Int. 31 (2005) 487–494.

[15] F. Chen, L.H. Wu, E.L. Zhao, Introduction of colored glasses, Chemical Industry Press, Beijing, 2008.

[16] S.G. Wang, J.J. Han, M.Q. Gao, The application of ligand field theory on the analysis of chemical states of iron in glass, Glass 6 (2000) 1–3.

[17] C.W. Zhang, The structural analysis and coordination discussion on iron-ion tinting principle in iron oxide containing glass, Glass Enamel. 32 (2004) 38–46.

[18] T. Yamashita, P. Hayes, Analysis of XPS spectra of Fe^{2+} and Fe^{3+} ions in oxide materials, Appl. Surf. Sci. 254 (2008) 2441–2449.

[19] M. Omran, T. Fabritius, A.M. Elmahdy, N.A. Abdel-Khalek, M. El-Aref, A. Elmanawi, XPS and FTIR spectroscopic study on microwave treated high phosphorus iron ore, Appl. Surf. Sci. 345 (2015) 127–140.

[20] F.M. Wang, T.A. Shifa, P. He, Z.Z. Cheng, J.W. Chu, Y. Liu, Z.X. Wang, F. Wang, Y. Wen, L.R. Liang, J. He, Two-dimensional metal phosphorus trisulfide nanosheet with solar hydrogen-evolving activity, Nano Energy 40 (2017) 673–680.

[21] M.T. Edmonds, A. Tadich, A. Carvalho, A. Ziletti, K.M. O'Donnell, S.P. Koenig, D.F. Coker, B. Özyilmaz, A.H. Castro Neto, M.S. Fuhrer, Creating a stable oxide at the surface of black phosphorus, ACS Appl. Mater. Inter. 7 (2015) 14557–14562.

[22] P. Luka, M.P.F. Graca, S. Zeljko, M.M. Andrea, M.A. Valente, Magnetic properties of iron phosphate glass and glass-ceramics, J. Am. Ceram. Soc. 97 (2014) 2517–2524.

[23] P. Bergoa, W.M. Pontuschkaa, J.M. Prison, Dielectric properties of P$_2$O$_5$–Na$_2$O–Li$_2$O glasses containing WO$_3$, CoO or Fe$_2$O$_3$, Solid State Commun. 141 (2007) 545–547.

[24] H.L. Lv, X.H. Liang, Y. Cheng, H.Q. Zhang, D.M. Tang, B.S. Zhang, G.B. Ji, Y.W. Du, Coin-like α-Fe$_2$O$_3$@CoFe$_2$O$_4$ core-shell composites with excellent electromagnetic absorption performance, ACS Appl. Mater. Inter. 7 (2015) 4744–4750.

[25] Y.Z. Zhao, H.R. Yin, Glass Technology, Chemical Industry Press, Beijing, 2006.

[26] J.D. Forster, H. Noh, S.F. Liew, V. Saranathan, C.F. Schreck, L. Yang, J.G. Park, R.O. Prum, S.J. Mochrie, C.S. O'Hern, H. Cao, E.R. Dufresne, Biomimetic isotropic nanostructures for structural coloration, Adv. Mater. 22 (2010) 2939–2944.

[27] S.G. Romanov, T. Maka, C.M. Sotomayor Torres, Diffraction of light from thin-film polymethylmethacrylate opaline photonic crystals, Phys. Rev. E. 63 (2001) 056603.